Al-Rafidain Engineering Journal (AREJ) Vol. 31, No. 1, March 2026, pp. 49-68

Energy, Economic, and Environmental Performance Analysis of a Perforated-Air PV/T Solar Collector with Variable Airflow During Winter in Zakho/Iraq

✉**Fatma Muhammed Khither*** fatmamuahammed721@gmail.com

Omar Mohammed Ali** omar.ali@uoz.edu.krd

* Mechanical Engineering Department, College of Engineering, University of Zakho Zakho, Iraq
*Engineering Research Center, University of Zakho, Zakho, Iraq.
** Mechanical Engineering Department, College of Engineering, University of Zakho Zakho, Iraq

Received: July 7th 2025 Received in revised form: August 16th 2025 Accepted: October 28th 2025

ABSTRACT

This study presents an experimental investigation of a perforated-air photovoltaic/thermal (PV/T) solar collector operating under variable airflow conditions during winter in Zakho, Iraq. The system integrates a perforated absorber plate with controlled airflow to enhance heat transfer and energy utilization. Three mass flow rates (0.055, 0.098, and 0.154 kg/s) were tested on separate winter days and compared to a conventional PV system. The results showed that the PV/T system significantly improved thermal efficiency, reaching up to 79.7%, while maintaining electrical efficiency between 12.7–13%. The highest useful thermal energy output was achieved at 0.154 kg/s, driven by improved convective heat transfer and favorable solar conditions. Despite slightly lower electrical efficiency than the PV panel, the PV/T system provided a much higher total energy yield. Economic analysis revealed that the PV/T system achieved up to five times higher Net Present Value (NPV) and a payback period of 1.6 years, with a lower Levelized Cost of Electricity (LCOE) of $0.16/kWh, compared to $0.1967/kWh for the PV system. Environmentally, the hybrid system reduced CO_2 emissions by over 68,000 kg over 25 years, approximately four times more than the PV system. The results confirm that the perforated-air PV/T system is a highly efficient and sustainable solution for cold-climate residential energy applications.

Keywords: *PV/T system, Perforated plate, Variable airflow, Thermal efficiency, CO_2 Emission reduction,*

https://jamh.uomosul.edu.iq/index.php/arej/index
Email: alrafidain_engjournal3@uomosul.edu.iq

==========

1. INTRODUCTION

The rapid growth of renewable energy, especially solar energy, is driven by the depletion of fossil fuels and environmental concerns. Globally, solar power capacity exceeded 480 GWp by the end of 2018, becoming the second-largest renewable source[1]. Photovoltaic (PV) systems convert solar radiation into electrical energy and can be combined with thermal collectors to provide heating and power, reducing overall energy consumption in residential and commercial settings[2].

In Iraq, despite its vast oil and gas resources, the energy sector faces persistent electricity shortages, aging infrastructure, and inefficiencies leading to frequent outages, especially during peak seasons. Most electricity generation relies heavily on fossil fuels, contributing to greenhouse gas emissions and environmental degradation [3], [4]. However, with average solar irradiance above 5 kWh/m²/day and more than 300 sunny days annually, Iraq has significant potential for solar energy deployment to enhance energy security and sustainability [5].

Photovoltaic/thermal (PV/T) systems, which integrate PV modules with thermal collectors, simultaneously generate electricity and useful heat. Since PV efficiency drops as cell temperature rises, effective cooling through heat transfer to a working fluid is essential to maintain performance [6]. Air-based PV/T collectors offer the advantages of simplicity and low cost, with configurations varying between single-pass and double-pass airflow and active or passive operation modes.

Several experimental studies have investigated these concepts. At Politecnico di Milano, Aste et al.[7] experimentally studied a

PV/T air collector and found that while PV electrical efficiency decreased at high cell temperatures during summer, the system's thermal performance improved with outlet air temperatures above 40°C. This improvement demonstrates the trade-off between electrical output and useful heat gain in PV/T systems under hot conditions.

Enhancing heat transfer between air and absorber plates is key to improving system efficiency. Techniques such as impinging air jets have shown improvements over conventional parallel flows[8]. Among these, perforated absorber plates have gained attention for their ability to promote turbulence by allowing airflow through distributed holes, thereby disrupting thermal boundary layers, enhancing convective heat transfer, reducing PV cell temperature, and increasing both thermal and electrical output [9].

Bizzy et al. [10] conducted an experimental study in South Sumatra, Indonesia, it was discovered that the use of perforated aluminum plates significantly enhanced the temperature and current-voltage output of 100 Wp poycrystalline solar panels. These findings underscore the significance of cooling in enhancing of photovoltaic efficiency in regions with high solar radiation.

Brideau and Collins [11] studied a hybrid PV/T solar collector with impinging jets for improved heat transfer. They used an aluminum-prickle plate for convective heat transfer. The results showed good agreement with experimental data, with predicted thermal and electrical outputs being 10% and 11% lower than expected. Kim & Yu. [12] conducted outdoor experiments on an air-type PVT collector with perforated baffles, emphasizing the significance of exergy analysis in conjunction with conventional energy analysis. The findings underscored the necessity of critical factors in the design of PVT systems, including enhanced thermal efficiency, reduced temperature differences, and improved ventilation.

Fterich et al. [13] studied on a PV/T air collector, in Sfax, Tunisia. They found that increasing the mass flow rate and input air velocity from 2 m/s to 3 m/s reduced the maximum temperature of the PV panel, thereby enhancing its thermal efficiency. Mazón-Hernández et al. [14] An experimental investigation was conducted at the Universidad Politécnica de Cartagena to enhance the efficiency of photovoltaic panels using of both forced and natural convection. They discovered that chilling caused a 0.4-0.5% decrease in electrical efficiency per degree increase in temperature. Additionally, they determined that forced air ventilation was superior to natural convection, underscoring the significance of ventilation in the design of PV systems. Baklouti & Driss [15] studied the PVT-air system's efficiency and revealed that higher airflow increases thermal efficiency, while the electricity output remaines unaffected.

Smaller ducts also improved thermal performance. The findings underscore the need for optimizing these parameters to enhance PVT-air system efficiency.

Prior research on PV/T air collectors has predominantly concentrated on traditional duct configurations, fixed airflow rates, and thermal improvement methods, frequently overlooking economic and environmental assessments. Research seldom examines the influence of variable airflow regulation, especially in cold-climate settings like Zakho in winter.

Experimental investigations on perforated-air PV/T systems are limited, primarily focusing on single-layer perforated configurations with static airflow, which neglects the advantages of dual air-gap designs created by horizontal internal perforated plates. The synergistic effects of variable airflow regulation and perforated absorber design during actual cold-season conditions in Northern Iraq are mostly unexamined.

This research intends to address these deficiencies by empirically assessing an innovative perforated-air PV/T solar collector with modifiable airflow under real winter climatic conditions in Zakho, Iraq. The goals are to measure enhancements in electrical and thermal performance relative to traditional systems. Evaluate the economic viability of the proposed system. Assess the ecological advantages, encompassing potential reductions in CO_2 emissions, and offer pragmatic suggestions for the implementation of such systems in frigid yet sunlit areas.

2. EXPERIMENTAL PROCEDURE

The experimental system was installed on the roof of the president building at the University of Zakho, Iraq, at a fixed tilt angle of 37° [16], corresponding to the site's latitude to optimize solar radiation capture (Figure.1). Figure 2 shows the average hourly temperature in the winter in Zakho, illustrating the typical ambient conditions during the experiment.

The experiment consists of two monocrystalline photovoltaic (PV) panels rated at 100 W each; one as a reference panel (PV) and the other integrated with a thermal collector to form a photovoltaic-thermal (PVT) system. The technical specifications of the monocrystalline PV panels are listed in Table 1.

Fig. 1. Solar PV panel and PVT systems.

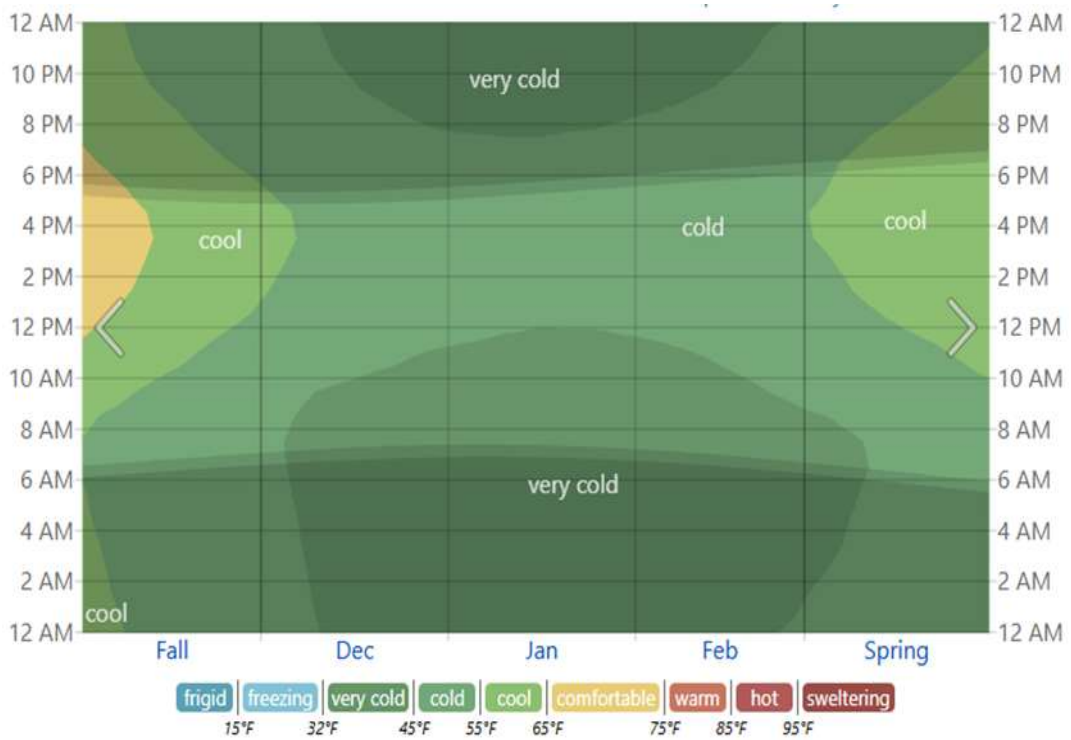

Fig.2 the average hourly temperature in the winter in Zakho.

The thermal collector was constructed as a three-layer structure, consisting of outer and inner layers of film-faced birch plywood with foam insulation in between. The collector's overall dimensions are 120 cm × 65 cm × 10 cm. A 1 mm-thick perforated aluminum plate (65 cm × 100 cm) was positioned at the center of the duct, as illustrated in Figure 3. This plate contains 322 circular holes, each 6 mm in diameter and spaced 42 mm apart (center to center), to enhance convective heat transfer within the airflow. Heat transfer between the PV cell and the perforated plate occurs predominantly via convection through the air stream, with negligible conduction due to the lack of direct physical contact. Temperature measurements were conducted using 19 digital thermometers (DS18B20 sensors). Six sensors were mounted on each panel: three on the rear surface and three on the front surface, arranged diagonally to capture temperature distribution, as shown in Figure 4(a). Additional sensors were installed at the air inlet, air outlet, and on the surface of the perforated plate, as shown in Figure 4(b). To ensure measurement reliability, all DS18B20 sensors were calibrated against a mercury thermometer over a temperature range of 0 °C to 100 °C. The calibration results showed excellent linear agreement, as presented in Figure 5, confirming the sensors' accuracy within ±0.2 °C.

Each system was connected to a 200 W aluminum shell resistor, which served as an electrical load to simulate energy consumption and allow for performance evaluation under operating conditions. Solar irradiance was measured using a YGC-JYZ pyranometer (range: 0–1500 W/m², accuracy: ±5%), and wind speed was recorded using a digital anemometer. Voltage and current were monitored using a DC voltage sensor and an ACS712 current sensor, respectively. Data acquisition was managed using an Arduino UNO microcontroller. A micro-SD card module, along with a DS1302 real-time clock (RTC), was employed to log current, voltage, temperature, wind speed, and solar radiation values for subsequent analysis.

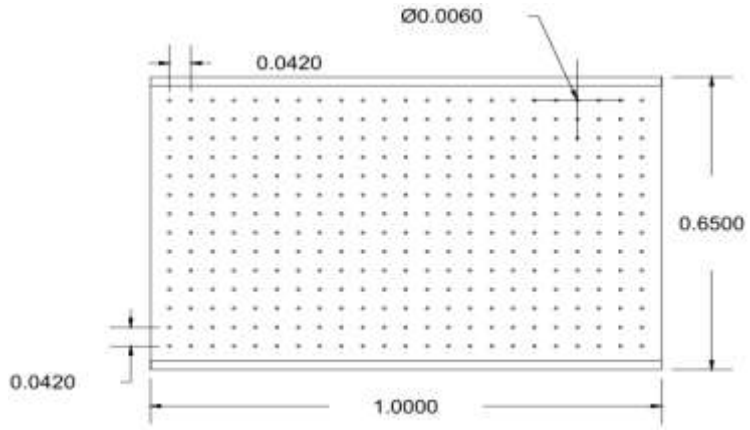

(a)

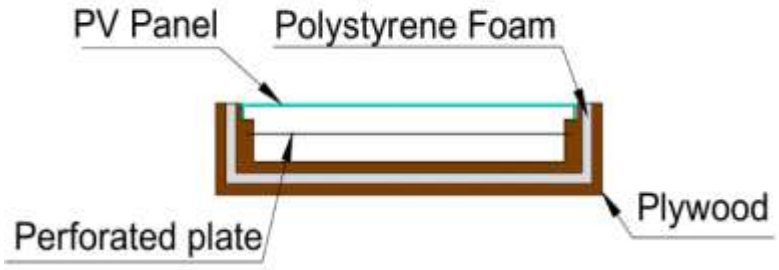

(b)

Fig. 3. (a) Perforated plate and (b) Cross-sectional schematic of the PV/T system.

The uncertainty analysis of the experimental measurements was conducted using the root-sum-square (RSS) method to estimate how measurement errors propagate into the final performance indicators. The analysis covers useful thermal power, photovoltaic power, thermal efficiency, and electrical efficiency. In this study, the air density and duct cross-sectional area were considered constant due to stable environmental conditions and fixed design [17].

The accuracy of the instruments used in this study is as follows: air velocity was measured with an accuracy of ±0.1 m/s; the temperatures at the air inlet and outlet were recorded with an accuracy of ±0.2 °C; voltage and current measurements had accuracies of ±0.05 V and ±0.05 A, respectively; and solar irradiance was measured with an accuracy of ±1 W/m².

The relative uncertainty in useful thermal power Q_{th} is calculated using:

$$\omega_{Q_{th}} = \left[\left(\frac{\partial Q_{th}}{\partial v}.\omega_v\right)^2 + \left(\frac{\partial Q_{th}}{\partial T_{in}}.\omega_{T_{in}}\right)^2 + \left(\frac{\partial Q_{th}}{\partial T_{out}}.\omega_{T_{out}}\right)^2\right]^{0.5} \quad (1)$$

The uncertainty in photovoltaic power P_{el} is given by:

$$\omega_P = \left[\left(\frac{\partial P}{\partial V}.\omega_V\right)^2 + \left(\frac{\partial P}{\partial I}.\omega_I\right)^2\right]^{0.5} \quad (2)$$

Thermal efficiency $\eta_{th}$was calculated as the ratio of useful thermal power to the incident solar power, and its uncertainty was estimated as:

$$\frac{\delta\eta_{th}}{\eta_{th}} = \sqrt{\left(\frac{\delta Q_{th}}{Q_{th}}\right)^2 + \left(\frac{\delta G}{G}\right)^2} \quad (3)$$

Table 1: PV panel characteristics.

Parameter	**Specification**
Type	Monocrystalline
Dimensions	1030 mm × 670 mm × 30 mm
Maximum Power (Pmax)	100 W
Open Circuit Voltage (Voc)	21.7 V
Short Circuit Current (Isc)	6.57 A
Cell Type	36 cells (4×9)
Maximum Power Voltage (Vmp)	18 V
Maximum Power Current (Imp)	5.56 A
Frame(material/color)	Anodized aluminum alloy/Silver
Front cover (material/thickness)	Low-iron tempered glass/3.2 mm
Operating Temperature Range	-4__85 °C
Power Tolerance	±3 %
Panel Efficiency	16.93 %

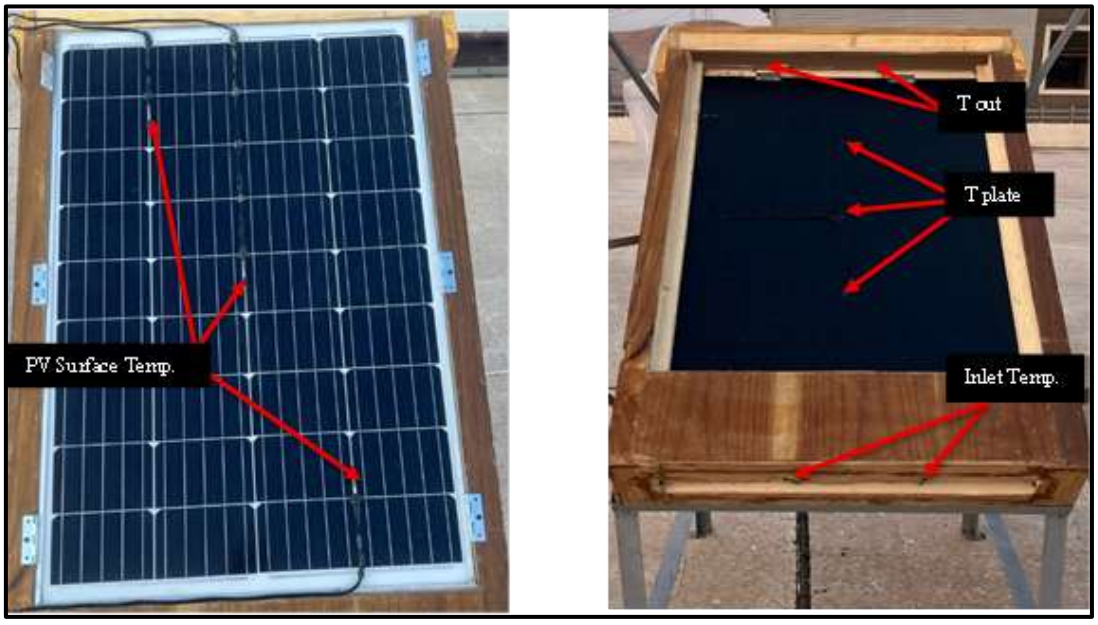

Fig.4 Temperature sensor's location.

Similarly, electrical efficiency η_{el} was calculated using electrical output and solar input, and its uncertainty is given by:

$$\frac{\delta\eta_{el}}{\eta_{el}} = \sqrt{\left(\frac{\delta V}{V}\right)^2 + \left(\frac{\delta I}{I}\right)^2 + \left(\frac{\delta G}{G}\right)^2} \quad (4)$$

By solving equations, the resulting uncertainties were determined as follows:

Useful thermal power	$\omega_{Q_{th}} = \pm 3.51\%$
Thermal efficiency	$\omega_{\eta_{th}} = \pm 3.51\%$
Photovoltaic power	$\omega_P = \pm 1.32\%$
Electrical efficiency	$\omega_{el} = \pm 1.33\%$

3. THEORETICAL BACKGROUND

The thermal and electrical performance of the air-based photovoltaic thermal (PVT) system was evaluated using an energy balance approach. The total solar energy incident on the collector was partitioned into electrical energy output, useful thermal energy gained by air, and thermal losses to the environment. The general energy balance can be expressed as [18]:

$$G.A = P_{el} + Q_{th} + Q_{loss} \quad (5)$$

Where:

- G: solar irradiance (W/m²)
- A: collector aperture area (m²)
- P_{el} : electrical output (W)
- Q_{th}: useful thermal energy output (W)
- Q_{loss}: total thermal losses to the environment (W)

The useful thermal energy is the amount of heat gained by the air as it passes through the collector due to the absorbed solar energy[19].

$$Q_{th} = \dot{m}.C_p.(T_{out} - T_{in}) \quad (6)$$

$$\dot{m} = \rho \cdot A_{duct} \cdot \dot{V} \quad (7)$$

Where:

- $\dot{m}$ mass flow rate of air (kg/s)
- Cp: specific heat capacity of air ≈ 1005 J/kg·K
- Tin, Tout: inlet and outlet air temperatures (°C)
- ρ: air density ≈ 1.2 kg/m³
- V: air velocity in the duct (m/s)

The electrical output is the solar energy converted into electricity by the PV panel, calculated from the measured current and voltage[20].

$$P_{el} = V.I \quad (8)$$

Where:

- V: voltage output from the PV panel (V)
- I: current output from the PV panel (A)

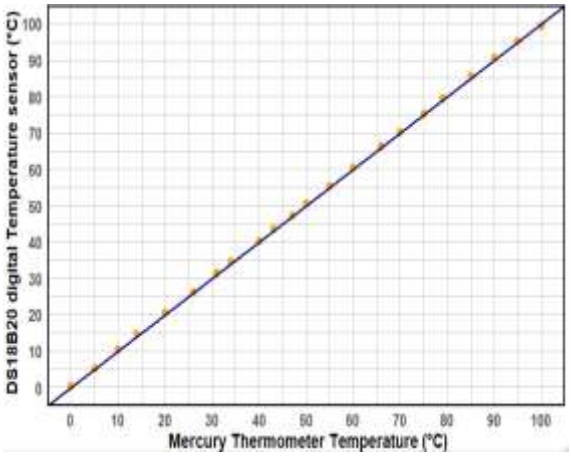

Fig. 5 Calibration of DS18B20 sensor against mercury thermometer.

Thermal losses from the absorber surface to the environment are given by[19]:

$$Q_{loss} = h_{loss}.A.(T_{pl} - T_a) \quad (9)$$

Where:

- h_{loss}: overall heat transfer coefficient (W/m²·K)
- T_{pl}: absorber plate temperature (°C)
- T_a: ambient temperature (°C)

The overall heat transfer coefficient (h_{loss}) is a sum of the convective heat transfer coefficient (h_{conv}) and the radiative heat transfer coefficient (h_{rad})[19]:

$$h_{loss} = h_{conv} + h_{rad} \quad (10)$$

This coefficient accounts for both the convective and radiative losses from the collector surface to the surrounding environment.

The convective heat transfer coefficient (h_{Conv}) due to wind over an external surface is a critical parameter in the estimation of heat losses or gains in solar energy systems. For outdoor surfaces, h_C is primarily influenced by wind speed and surface orientation. An empirical correlation widely accepted in the literature for horizontal or vertical flat surfaces is given by[19]:

$$h_{Conv} = 5.7 + 3.8\,V_{wind} \quad (11)$$

Where:

- h_{Conv} is the convective heat transfer coefficient (W/m²·K),
- V_{wind} is the wind speed in the vicinity of the surface (m/s).

This relation, recommended by ASHRAE and used in various solar thermal applications, accounts for both natural and forced convection components. The constant term (5.7) represents natural convection under still air conditions, while the second term accounts for the enhancement due to wind-driven forced convection.

The radiative heat transfer coefficient is calculated using the Stefan-Boltzmann law[19]:

$$h_{rad} = \varepsilon.\sigma.\left({T_{pv}}^2 + {T_{sky}}^2\right).\left(T_{pv} + T_{sky}\right) \quad (12)$$

Where:

- ε: Surface emissivity (typically 0.85–0.95)
- σ: Stefan–Boltzmann constant = $5.67 \times 10^{-8}\, W/m^2 \cdot K^4$
- T_{pv}: PV temperature in Kelvin
- T_{sky}: Sky temperature in Kelvin, approximated by:

$$T_{sky} = T_a - 6℃$$

The efficiencies of the PV/T system can be evaluated as follows:

Thermal Efficiency which represents the proportion of incoming solar energy converted into thermal energy[21].

$$\eta_{th} = \frac{Q_{th}}{G \cdot A} \quad (13)$$

Electrical Efficiency which represents the proportion of incoming solar energy converted into electricity[20]

$$\eta_{el} = \frac{Q_{el}}{G \cdot A} \quad (14)$$

The total efficiency combining both electrical and thermal efficiencies.

$$\eta_{overall} = \eta_{el} + \eta_{th} \quad (15)$$

4. ECONOMIC AND ENVIRONMENTAL ANALYSIS

4.1 Economic Analysis

This section evaluates the economic performance of the perforated-air PV/T solar collector by analyzing the system's capital and operational costs, annual energy production, annual revenue, net present value (NPV), payback period, and levelized cost of electricity (LCOE). This approach ensures a comprehensive understanding of its financial feasibility.

Capital and Operational Costs:

These include the initial investment needed to build the system and the recurring costs for operating and maintaining it annually. Capital costs are one-time expenses, while operational costs are incurred throughout the system's life[22].

- Capital Cost (C_0):

$$C_0 = C_{PV} + C_{thermal} + C_{blower} + C_{structure} + C_{installation} + C_{inverters} \quad (16)$$

Where:

- C_0: Total capital cost of the system.
- C_{PV}: Cost of the photovoltaic (solar) panels.
- $C_{thermal}$: Cost of thermal collector components.
- C_{blower}: Cost of the centrifugal blower used for air circulation.
- $C_{structure}$: Cost of structural materials and framing.
- $C_{installation}$: Labor and installation expenses for setting up the system.
- $C_{inverters}$: Cost of inverters.

- Annual Operational Cost (C_{OP}):

$$C_{OP} = C_{maintenance} + C_{blower\ energy} \quad (17)$$

Annual Energy Production represents the total useful energy generated by the system annually, combining both electrical output and the thermal energy converted into its electrical equivalent.

$$E_a = \eta_{sys} \cdot A_{PV} \cdot G \cdot N \quad (18)$$

Where:

- N: Number of days during the year
- G: Global irradiance.
- η_{sys}: System efficiency
- A_{PV}: Area of PV Panel

Daily consumption for space heating:

$$Q_{heating} = U * A_{Floor} * HDD * \frac{24}{1000} \quad (19)$$

- U: overall heat transfer coefficient ($W/m^2 \cdot K$)
- A_{Floor}: Area of floor (m^2)
- HDD: Heating degree day ($°C.day$)

Annual Revenue (R) is the financial return obtained from the energy generated by the system, either through energy savings or income from selling electricity[22]:

$$R = E_a \times C_{elec} \quad [\text{USD/year}] \quad (20)$$

Where:

- C_{elec} Cost of electricity per kWh (as avoided grid electricity or feed-in tariff).

Net Present Value (NPV) is used to evaluate the long-term profitability of the system by calculating the present value of future cash flows, discounted over time[23].

$$NPV = \sum_{t=1}^{n} \frac{C_t}{(1+r)^t} - C_0 \quad (21)$$

Where:

- Ct: Cash inflow in year
- n: system lifetime (years)
- r: discount rate

Simple Payback Period (SPP) indicates the time required for the system to recover its initial investment from the net annual revenue.

$$Payback\ Period = \frac{Initial\ Investment}{Annual\ Cash\ Flow\ (Net\ Savings)} \quad (22)$$

Levelized Cost of Electricity (LCOE) is the average cost per unit of electricity generated over the lifetime of the system, providing a basis for comparing with other energy sources[24].

$$\text{LCOE} = \frac{\text{Total Lifetime Costs}}{\text{Total Lifetime Electricity Generated}} = \frac{\sum_{t=1}^{N} \frac{C_t + C_{OP}}{(1+r)^t}}{\sum_{t=1}^{N} \frac{E_t}{(1+r)^t}} \quad (23)$$

Where:

- C_t: Capital expenditure in year t (e.g., initial investment or replacement costs)
- C_{OP}: Operating and maintenance costs in year t
- Et: Energy produced in year t
- r: Discount rate (representing the time value of money)
- N: Lifetime of the project in years.

4.2 Environmental Analysis

The environmental performance of the PV/T system is evaluated by estimating the reduction in greenhouse gas emissions due to the displacement of conventional electricity sources.

The amount of avoided CO_2 emissions is calculated based on the emission factor of the local electricity grid[25].

$$CO_2\_saved = E_a \times EF \quad [kWh/year] \quad (24)$$

Where:

- E_a is the annual energy produced by the system $[kWh/year]$.
- EF is the CO_2 emission factor of grid electricity $[kg\ CO_2/kWh]$.

Total Emission Savings Over System Lifetime:

$$Total\ CO_2 saved = CO_2\ saved \times n \quad (25)$$

Where n is the lifetime of the system in years.

This shows the system's potential to contribute to climate change mitigation by reducing reliance on fossil-fuel-generated electricity. The CO_2 emission reduction was estimated using an emission factor of 0.9247 kg CO_2/kWh for grid electricity[25].

5. RESULTS AND DISCUSSION

This section presents and analyzes the experimental and economic performance of the PV/T system under varying operating conditions. The system was tested on three separate days with different mass flow rates and environmental conditions. The results are categorized into three parts: technical results, economic evaluation, and environmental performance. The goal is to assess the feasibility of PV/T technology in terms of thermal and electrical behavior, long-term economic return, and environmental benefits compared to a conventional PV system.

5.1 Technical results

The technical performance of the PV/T system was analyzed through parameters such as solar radiation, ambient temperature, wind velocity, surface temperature, outlet air temperature, useful thermal energy output, and electrical efficiency.

Figure 6.a shows the variation in solar radiation throughout the day. On 09 February, solar radiation started at approximately 480 W/m² at 09:00, peaked at 1005 W/m² around 13:00, and declined to 540 W/m² by 16:00. On 15 February, radiation began slightly higher at 510 W/m², reached the maximum observed value of 1056.89 W/m² at 13:00, and dropped steadily through the afternoon. On 18 February, the curve followed a similar pattern, with a peak of 1035 W/m² at 13:30. This consistent midday peak corresponds to the sun's highest position and clear-sky conditions.

Figure 6.b presents the ambient temperature profiles. On 09 February, the temperature began at 10.7 °C, peaked at 19.3 °C, and ended at 17.8 °C, indicating a relatively cool day. On 15 February, the ambient temperature ranged from 13.1 °C to 22.6 °C. While on 18 February, it was the highest overall, starting at 14.1 °C and peaking at 27 °C. The progressive rise in ambient temperature enhances the air's heat-absorbing capacity, which improves thermal performance. However, higher ambient temperatures also raise the PV surface temperature, reducing electrical efficiency.

Figure 6.c illustrates the wind velocity profiles throughout the day. On 09 February, the wind speed was highest, starting at 5.4 m/s at 09:00, and gradually declining during the day. 15 February data showed more stable but moderate wind, peaking at 3.2 m/s at 08:30. 18 February had the lowest and most stable wind speeds, reaching a maximum of 4.1 m/s. The stronger early wind on09 February contributed to passive cooling of the PV/T surface, which helped mitigate thermal stress and maintain better electrical efficiency despite lower irradiance.

Figure 7 presents the outlet air temperature (Tout) under varying mass flow rates (0.055 kg/s, 0.098 kg/s, and 0.154 kg/s). Across all

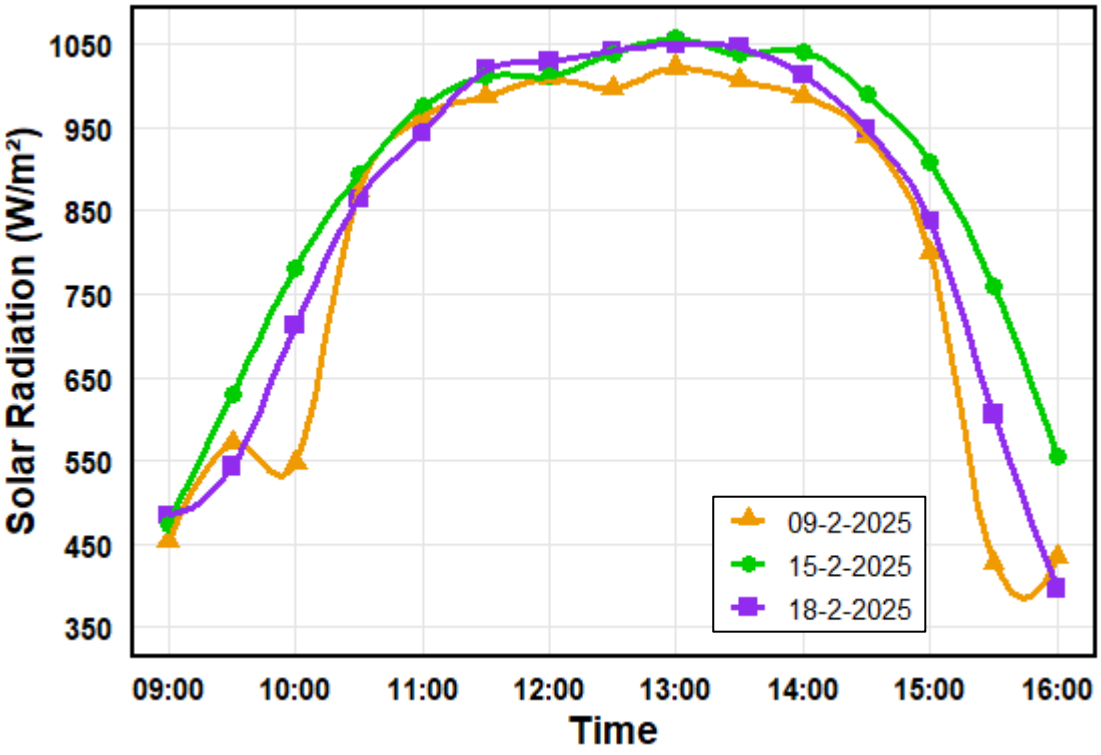
Solar Radiation (W/m²)
1050
950
850
750
650
550
450
350
09:00
10:00
11:00
12:00
13:00
14:00
15:00
16:00
Time
09-2-2025
15-2-2025
18-2-2025

(a)

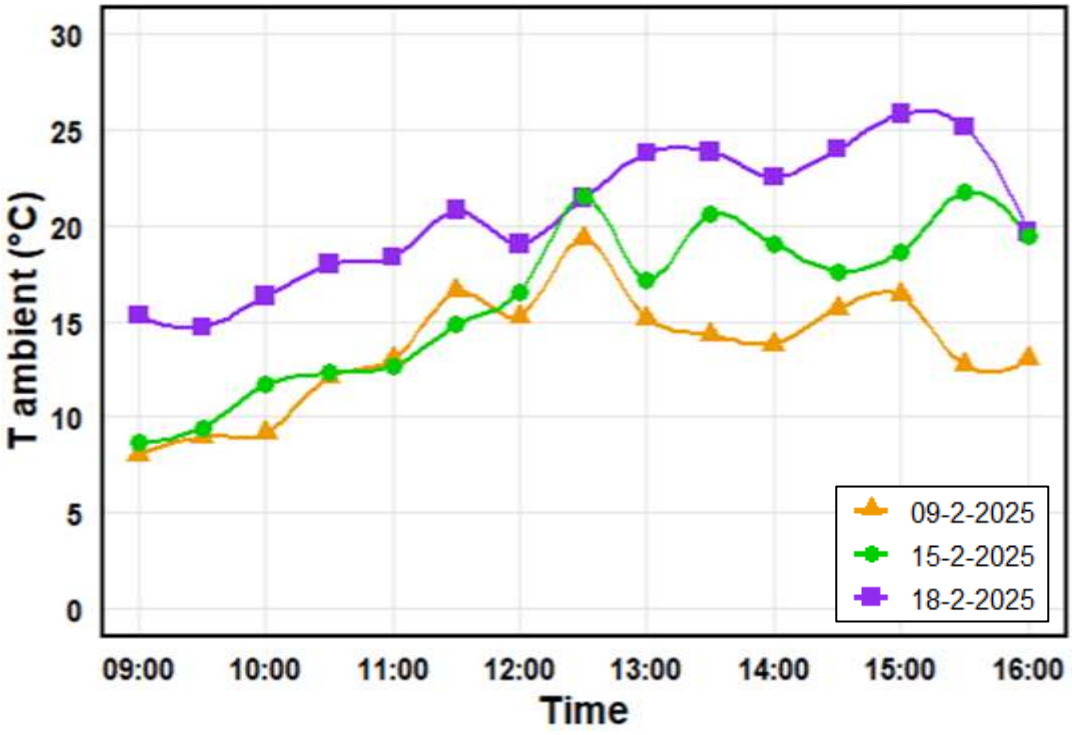
T ambient (°C)
30
25
20
15
10
5
0
09:00
10:00
11:00
12:00
13:00
14:00
15:00
16:00
Time
09-2-2025
15-2-2025
18-2-2025

(b)

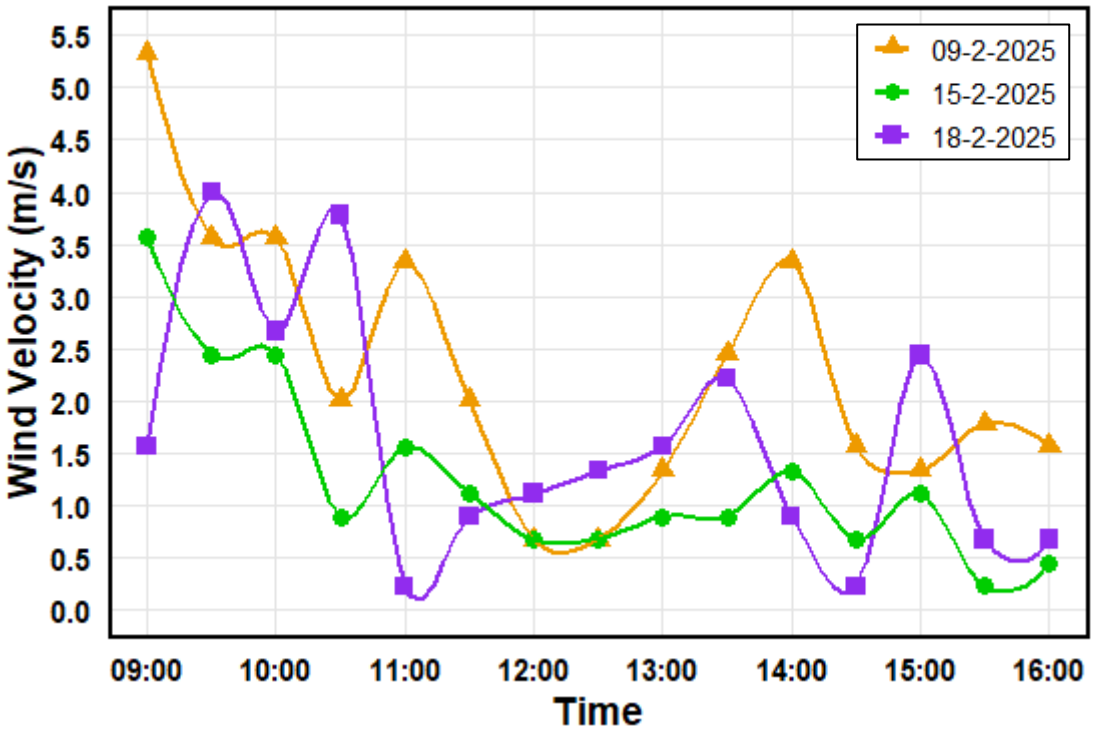

(c)

Fig. 6. Variation of (a) solar radiation, (b) ambient temperature, and (c) wind velocity with time for different days in February 2025.

test days, Tout followed a similar pattern, rising from morning to early afternoon in line with solar radiation, then gradually decreasing in the late afternoon. On 18 February ($\dot{m} = 0.098 kg/s$), Tout started at 14.6 °C, peaked at 35.1 °C at 13:30, and ended at 24.1 °C, the highest among all cases. This trend was primarily due to the high ambient temperature and strong solar irradiance on that day. On 15 February ($\dot{m} = 0.154 kg/s$), Tout peaked at 32.4 °C, while on 09 February ($\dot{m} = 0.055 kg/s$) (lowest ambient and solar radiation), it reached a maximum of only 28.3 °C. The outlet temperature was consistently lower at the highest airflow rate (0.154 kg/s), as the increased air velocity reduced residence time in the duct, resulting in a lower temperature rise despite higher heat extraction.

At the medium flow rate (0.098 kg/s), Tout was the highest overall, indicating a balanced interaction between airflow rate and heating time. Interestingly, the lowest Tout occurred at 0.055 kg/s (09 February), despite the longer residence time, due to insufficient solar radiation and cooler ambient air. This confirms that outlet air temperature is not determined by flow rate alone but is strongly influenced by the combined effects of solar irradiance, ambient temperature, and airflow.

Figure 8 presents the useful thermal energy output of the PV/T system for three days. On 09 February ($\dot{m} = 0.055 kg/s$), thermal energy started at 211 W, peaked at 508W, and ended at 197W. The lower output was due to lower irradiance, cooler ambient temperature, and high wind speed, which led to greater heat loss to the surroundings.

On 18 February ($\dot{m} = 0.098 kg/s$), output ranged from 254 W to 540 W, ending at 182W. Despite high ambient temperature and strong irradiance, the moderate airflow (0.098 kg/s) and lower wind speed limited the rate of heat extraction.

The highest performance occurred on 15 February ($\dot{m} = 0.154 kg/s$), when thermal output started at 237W, peaked at 587W, and ended at 291 W. This was due to the combination of maximum irradiance, high airflow, and moderate wind, which reduced convective heat losses and improved overall heat transfer.

These results confirm that thermal energy output is primarily driven by solar radiation and airflow, but also influenced by wind speed, which increases convective losses. Lower wind on 15 February helped retain more heat within the system, enhancing useful thermal gain.

Figure 9 shows the variation in PV/T surface temperature of the panel over three days. In all cases, the surface temperature increased until early afternoon and then decreased as solar radiation declined. On 09 February ($\dot{m} = 0.055$ kg/s), the surface temperature of the

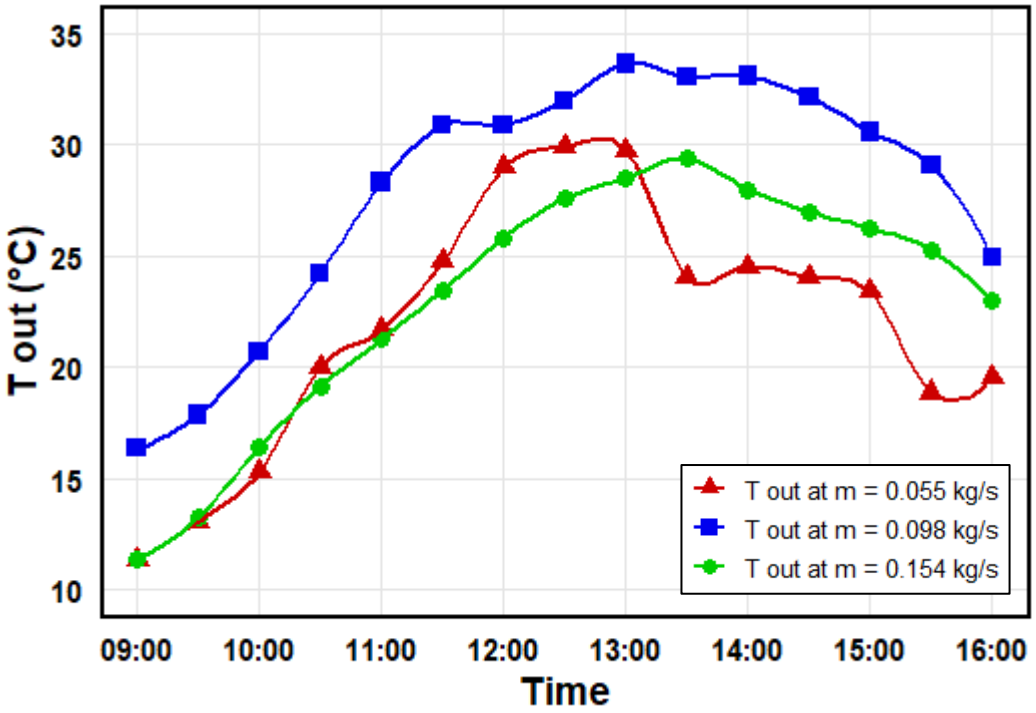

Fig.7 Outlet air temperature of the PV/T system over time at different airflow rates.

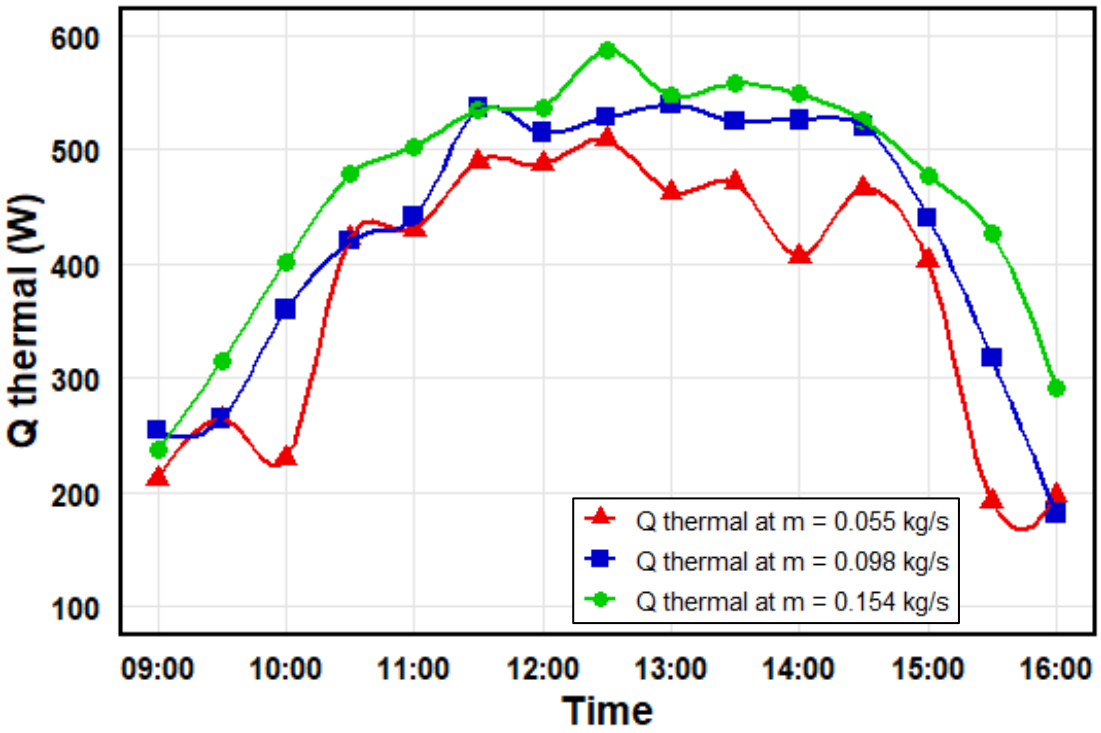

Fig.8 Useful thermal energy output from the PV/T system throughout the day for various airflow rate

panel ranged from 17.5 °C to 39.6 °C, ending at 25.1 °C. Despite the lowest airflow, surface temperature remained moderate due to lower solar radiation and the highest wind velocity (up to 5.4 m/s), which enhanced external convective cooling over the PV surface.

On 18 February ($\dot{m} = 0.098$ kg/s), the surface temperature of the panel was highest overall, rising from 22.2 °C to 43.5 °C and ending at 27.8 °C. This rise was driven by strong solar irradiance, high ambient temperature, and low wind speed, which limited external convective cooling of the front PV surface. At the same time, internal airflow through the duct was not sufficient to dissipate the absorbed heat fully. On 15 February ($\dot{m} = 0.154$ kg/s), the surface temperatures ranged from 18.1 °C to 41.0 °C, ending at 28.5 °C. The higher internal airflow (mass flow rate) through the duct combined with moderate wind speed enhanced both internal and external heat removal, resulting in better cooling of the PV surface compared to 18 February.

Figure 10 illustrates the electrical efficiency of the PV/T system across three days. For all cases, efficiency was highest in the morning and late afternoon, and lowest around midday due to rising surface temperature and solar irradiance.

On 09 February ($\dot{m} = 0.055$ kg/s), the efficiency started at 17.5%, dropped to 10.9%, and tthen recovered to 16.8% by 16:00. The cooler ambient conditions, lower irradiance, and strong wind speed (up to 5.4 m/s) provided excellent natural cooling, helping to reduce the PV surface temperature and maintain higher electrical efficiency despite low solar input. On 18 February ($\dot{m} = 0.098$ kg/s), the efficiency ranged from 16.8% to 10.3%, ending at 15.9%. Although irradiance was strong, low wind and higher surface temperatures reduced electrical performance, especially around midday.

On 15 February ($\dot{m} = 0.154$ kg/s), the efficiency ranged from 17.1% to 10.5%, ending at 16.5%. Despite high irradiance, the higher airflow rate improved internal cooling and reduced surface temperature more effectively than in the medium-flow case. These results show that the mass flow rate does influence electrical efficiency by regulating internal convective cooling. However, its effect is more pronounced when external cooling (via wind) is limited. Therefore, electrical efficiency is governed by surface temperature, which is affected by a combination of mass flow rate, ambient temperature, solar irradiance, and wind speed. The best overall performance occurred on 09 February, where strong wind and mild weather conditions minimized thermal stress on the PV module.

Figure 11 presents the daily average electrical and thermal efficiencies of both the reference PV system and the PV/T system over three experimental days.

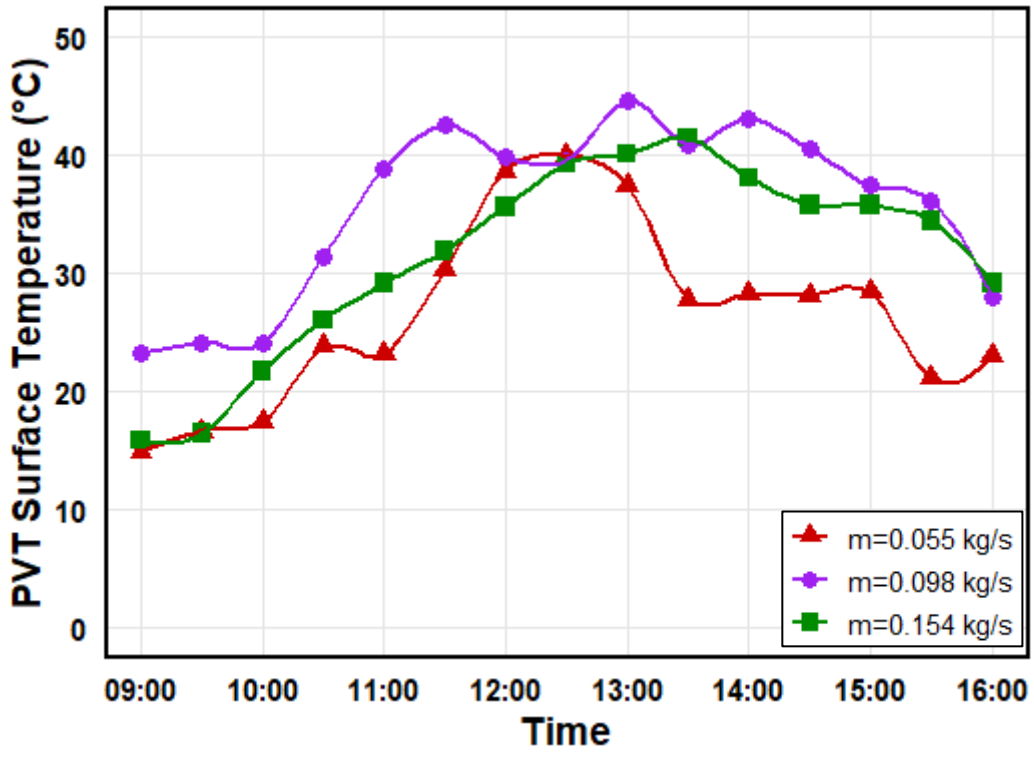

Fig.9 PV/T surface temperature of panel variation during the day under different airflow rates

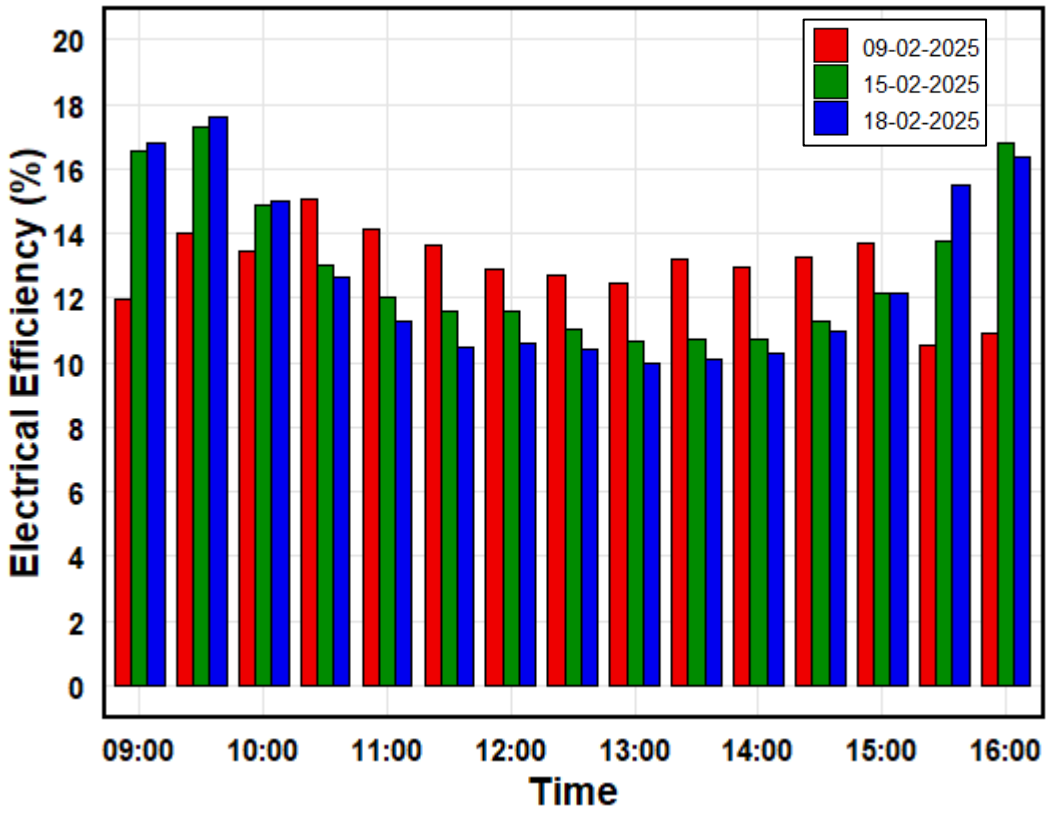

Fig. 10 Electrical efficiency of the PV/T system over time at varying mass flow rate.

The maximum efficiency observed approaches 80%. The relatively high thermal efficiency results from winter testing conditions with low ambient temperatures and high airflow, which minimized thermal losses and maximized useful heat gain.

On 09 February ($\dot{m}$ = 0.055 kg/s), the reference PV panel achieved an electrical efficiency of 14%, slightly higher than the PV/T system at 13%, while the thermal efficiency of the PV/T system reached 67.67%.

The higher electrical efficiency of the reference PV panel was attributed to favorable ambient conditions and strong wind, which enhanced convective heat loss from both its front and rear surfaces. In contrast, the rear surface of the PV/T panel was thermally insulated, limiting passive cooling and leading to slightly elevated surface temperatures.

On 15 February ($\dot{m}$ =0.154kg/s), electrical efficiencies were 14.2% (PV) and 12.9% (PV/T), while thermal efficiency peaked at 76.54% due to high solar irradiance and increased airflow through the PV/T duct. Nevertheless, the limited external convective cooling led to elevated PV surface temperatures and a minor drop in electrical performance.

On 18 February ($\dot{m}$ =0.098kg/s), the highest electrical efficiency was recorded for the reference PV panel (14.9%), while the PV/T system achieved 12.7%. Thermal efficiency remained high at 73.33%, but the low wind speed on that day reduced heat loss from the front surface, increasing PV module temperature and reducing electrical output. These results confirm that while the PV system maintained higher electrical efficiency due to better natural cooling, the PV/T system significantly enhanced thermal performance, offering improved total energy utilization.

To further illustrate the system performance, Table 2 presents the average electrical power, thermal power (Q thermal), and corresponding electrical and thermal efficiencies for the reference PV panel and the PV/T system under all three airflow cases.

The results highlight that, compared to the standalone PV module, the PV/T collector consistently achieved higher overall energy output due to the simultaneous production of electricity and useful thermal energy, with efficiency gains varying according to airflow rate.

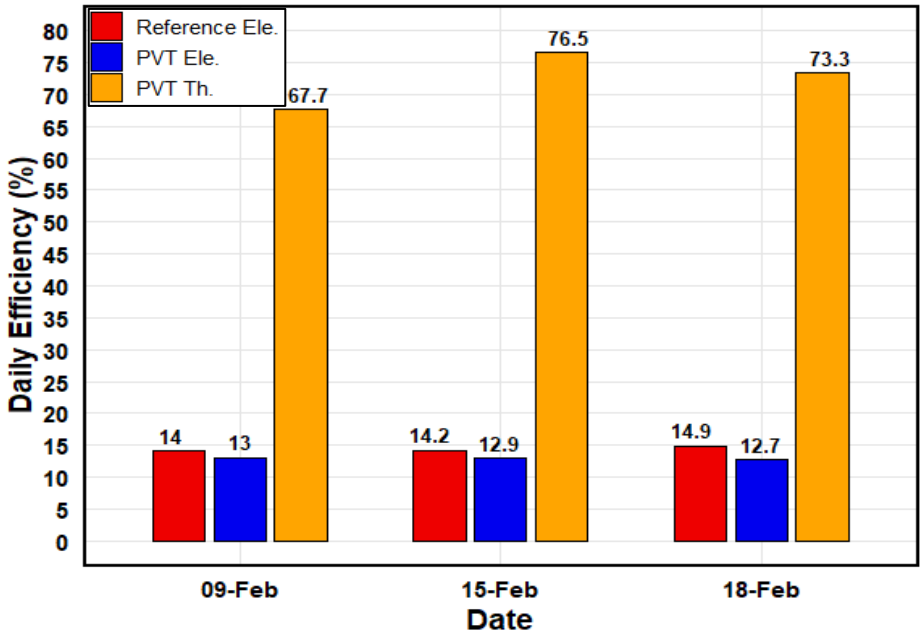

Fig. 11 Daily efficiency of the PV/T and PV system for different days in February 2025.

Table 2: Electrical and Thermal performance comparison of PV and PV/T systems.

Parameter	PV (Reference)	PV/T at $\dot{m}$ = 0.055 kg/s	PV/T at m = 0.098 kg/s	PV/T at m = 0.154 kg/s
Q (thermal)	--	401.4 W	448.91 W	484.98 W
Electrical power	77.62 W	72.75 W	69.15 W	75.46 W
Thermal efficiency	--	67.67%	73.33%	76.54%
Electrical efficiency	14.04%	12.99%	12.68%	12.93%

5.2 Economic results

This analysis consider two systems: PV and PV/T. Each one is alone for a typical residential house of 150 m², occupied by four people, each requiring approximately 5 kWh/day, resulting in a daily energy demand of 20 kWh, or 7,300 kWh annually[26]. The system under study was evaluated for its ability to meet this energy need while also maximizing economic return. Using the previously defined system efficiency equation, the required PV area (A_{pv}) was calculated to be approximately m² for the PV system and 31.54 m² for the PV/T system. These areas were determined based on the annual energy requirement, average solar irradiance, and actual system efficiency.

Additionally, the annual space heating demand for the house was estimated to be 2988 kWh/year, based on building size and winter heating needs. This thermal load highlights the benefit of the PV/T system, which not only provides electrical output but also significantly contributes to meeting heating requirements, thereby increasing total system effectiveness and return on investment.

The cost parameters used for the NPV and LCOE calculations are presented in Table 3. The system lifetime was assumed to be 25 years with a discount rate of 3% [27]. The electricity selling price was set at 0.183 USD/kWh, in line with local tariff rates [28].

Figure 12 presents the Net Present Value (NPV) progression over a 25-year lifetime for the reference PV system and three PV/T systems operating at airflow rates of 0.055 kg/s, 0.098 kg/s, and 0.154 kg/s. All PV/T configurations were sized to meet the total annual energy needs of the household, including electricity demand

(7,300 kWh/year) and space heating consumption (2,988 kWh/year), as outlined in Section 5.

In contrast, the reference PV system covers only the electrical load. The PV/T systems not only satisfied the electrical demand but also generated a significant surplus of thermal energy for space heating. Specifically, the 0.055 kg/s system delivered 20,118.5 kWh of useful heat, the 0.098 kg/s system produced 22,309.75 kWh, and the 0.154 kg/s system generated 22,312.14 kWh. This substantial thermal energy output exceeded the household heating demand, increasing energy savings and improving economic performance.

By year 25, the cumulative NPVs reached 17,512.22 USD for the reference PV system, 79,819.60 USD for the PV/T system at 0.055 kg/s, 86,800.35 USD at 0.098 kg/s, and 86,807.67 USD at 0.154 kg/s. Although the 0.154 kg/s system achieved the highest NPV, the difference from the 0.098 kg/s configuration was negligible (only about 7 USD), indicating similar financial viability. Therefore, airflow rate selection may be guided by technical factors such as fan size, system complexity, or thermal control requirements.

The NPV curves show a gradual rise in early years and a steeper increase toward the end of the project lifetime due to accumulated energy cost savings. The PV/T systems achieved much higher NPV values than the reference PV system because they generate both electricity and thermal energy. The reference PV system, while economically viable, showed significantly lower NPV compared to the PV/T systems, confirming the superior long-term value of hybrid systems in residential applications where both electricity and heat are utilized.

Table 3 provides a consolidated summary of the key economic and technical parameters for the reference PV system and PV/T systems at three different airflow rates. The overall capital expenditure for the PV/T systems is elevated due to the incorporation of a blower and thermal collector, rising from 5,750 USD(PV) to $7,550 (PV/T). This supplementary investment leads to a substantially higher energy output, with PV/T systems generating around 29,610.76 kWh/year, in contrast to 7,300 kWh/year from the sole PV system.

The PV/T systems exhibit a much lower Levelized Cost of Electricity (LCOE), ranging from 0.039 to 0.042 USD/kWh, in contrast to 0.071 USD/kWh for the reference PV, and provide considerably shorter payback times of about 1.6 to 1.7 years for PV/T systems compared to 4.5 years for the standalone PV system. The Net Present Value (NPV) findings over 25 years significantly improve, confirming the payback period outcomes and underscoring the long-term financial benefits

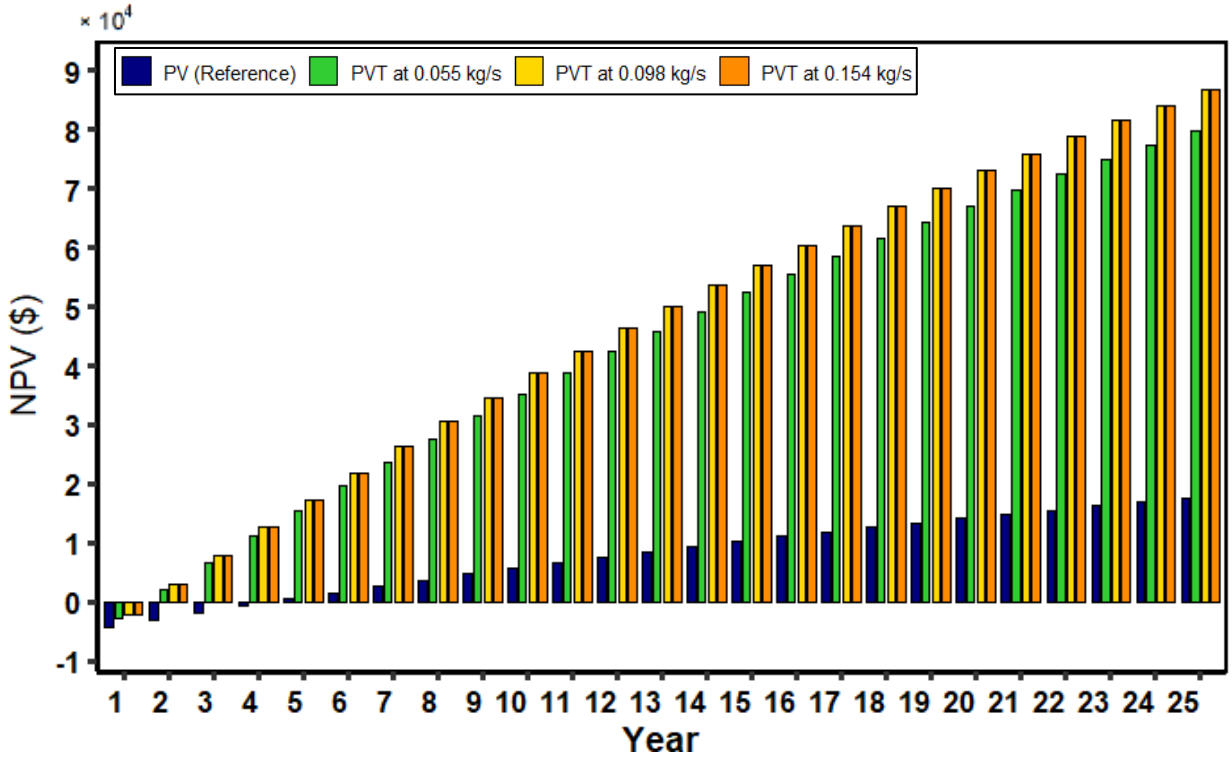

Fig. 12 the Net Present Value (NPV) over a 25-year lifetime for different systems and airflow rates

of hybrid systems. The global range of the Levelized Cost of Energy (LCOE) for residential solar systems is between 12.2 and 28.4 cents per kilowatt-hour for rooftop solar systems; thus, the LCOE values in the present study have been considered appropriate [29].

This table highlights that, despite slightly higher upfront costs, the PV/T systems are superior in terms of energy output, cost-effectiveness, and investment return, particularly for residential applications with both electrical and thermal demand.

5.3. Environmental Results

Figure 13 compares the total CO_2 emissions saved over a 25 environmental benefits year period by the reference PV system and PV/T systems at three different airflow rates. These calculations are based on the displacement of grid electricity, assuming an emission factor of 0.9247 kg CO_2 per kWh of electricity generated[25].

The reference PV system saved approximately 16,880 kg of CO_2 over its lifetime. In contrast, the PV/T systems achieved significantly higher environmental benefits: 63,380 kg saved at 0.055 kg/s, 68,450 kg at 0.098 kg/s, and 68,450 kg at 0.154 kg/s. The CO_2 savings for PV/T systems were approximately 4 times higher than those the standalone PV system, due to their ability to generate both electrical and thermal energy. The 0.098 and 0.154 kg/s systems achieved identical CO_2 reductions, reflecting their nearly equal total energy output. Even the lowest-flow PV/T configuration (0.055 kg/s) achieved a substantial reduction, making all three PV/T setups environmentally superior.

These results confirm that hybrid PV/T systems not only offer better technical and economic performance but also contribute significantly to emissions reduction, making them a strong candidate for sustainable residential energy applications.

6. CONCLUSION

This study experimentally evaluated the energy, economic, and environmental performance of a perforated-air PV/T solar collector under different airflow rates during winter in Zakho, Iraq. Based on the results, the following conclusions were drawn:

1. Higher thermal efficiency was achieved by the PV/T system, reaching up to 79.7% due to the enhanced convective heat transfer provided by increased airflow rates, particularly at 0.154 kg/s under strong solar radiation.
2. Electrical efficiency was consistent across various flow rates, despite a minor decrease compared to a standard PV panel as This was because the lower PV cell temperature from air cooling facilitated the maintenance of efficiency between 12.7% and 13%, while concurrently generating beneficial thermal energy

Table 3: Technical and economic comparison of PV and PV/T systems over 25 years.

Item	Value			
	PV (Reference)	PV/T at $\dot{m}$ = 0.055 kg/s	PV/T at m = 0.098 kg/s	PV/T at m = 0.154 kg/s
PV array	2500 USD	2500 USD	2500 USD	2500 USD
Inverter	1000 USD	1000 USD	1000 USD	1000 USD
Structure, installation	2250 USD	2250 USD	2250 USD	2250 USD
blower	0	300 USD	300 USD	300 USD
Thermal collector	0	1500 USD	1500 USD	1500 USD
Total	5750 USD	7550 USD	7550 USD	7550 USD
System Lifetime	25Years	25Years	25Years	25Years
Modules full area	27.7 m^2	30.79 m^2	31.54 m^2	30.93 m^2
Yielded Energy	7300kWh/year	27417.8kWh/year	29608.42kWh/year	29610.76kWh/year
NPV	17512.22 USD	79819.6USD	86800.35USD	86807.67USD
LCOE	0.071 USD/kWh	0.043 USD/kWh	0.039 USD/kWh	0.039 USD/kWh
Payback period	4.5 years	1.7 years	1.6 years	1.6 years

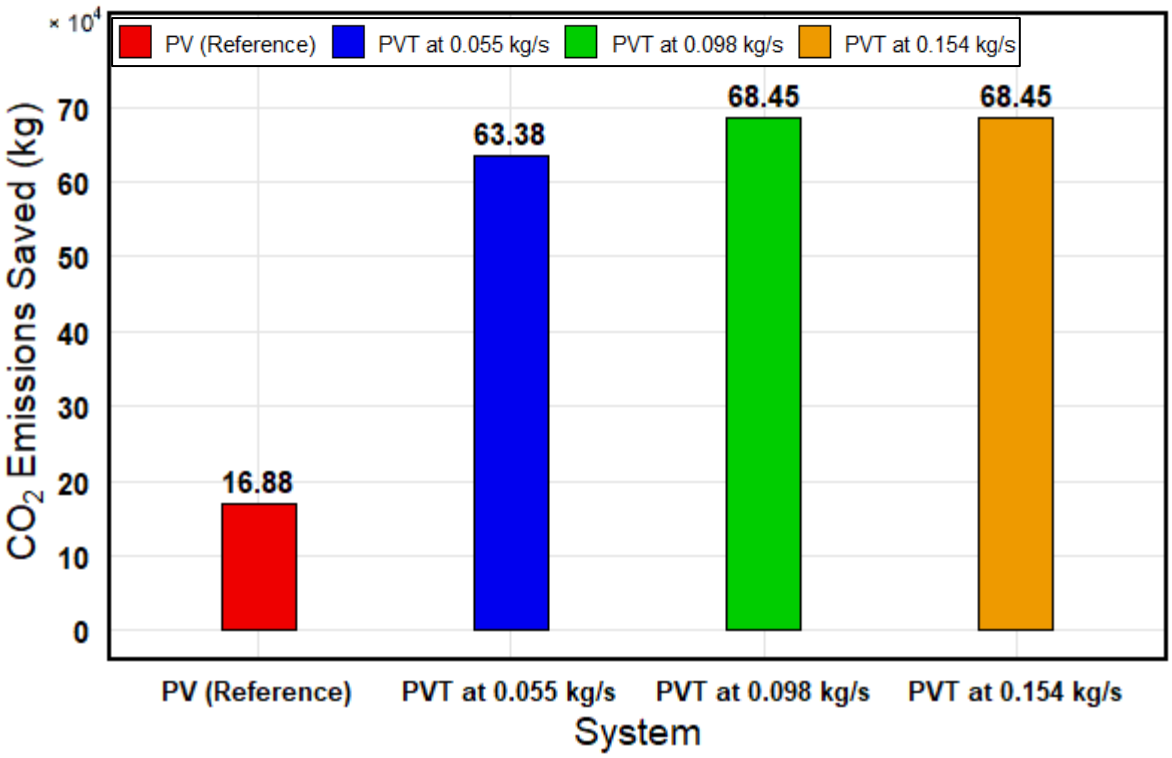

Fig.13 total CO_2 emissions saved over a 25-year lifetime for different systems and airflow rates

3. Total useful thermal energy output was maximized at higher airflow rates. The PV/T system with 0.154 kg/s airflow (On 15 February) produced maximum thermal output, indicating that increased flow enhances energy extraction, although at lower outlet temperatures.

4. Environmental conditions such as wind speed and ambient temperature influenced system performance. Higher wind velocities enhanced convective cooling, especially for the PV-only system, while lower ambient temperatures contributed to better electrical performance.

5. The PV/T system demonstrated superior economic performance compared to the reference PV system. It attained a Net Present Value (NPV) of $86,807, a payback period of 1.6 years, and a Levelized Cost of Electricity (LCOE) of $0.04/kWh, in contrast to the elevated LCOE and extended payback duration of the photovoltaic-only system.

6. The thermal output of the PV/T system satisfied and exceeded the space heating requirements. The system generated almost 22,300 kWh of heating energy, which greatly exceede the yearly heating requirement of 2,988 kWh, resulting in enhanced savings and a reduced payback period.

7. The PV/T system made a substantial contribution to the reduction of emissions. It reduced CO_2 emissions by about 68,000 kg over 25 years (four times the reference PV) due to its dual generation of energy and heat.

The perforated-air PV/T design, particularly at 0.154 kg/s, demonstrates a well-balanced, high-performance solution. It efficiently amalgamates technological, economic, and environmental advantages, rendering it appropriate for residential use in cold areas with heating requirements.

Nomenclature

T_{in}	Air inlet temperature, ℃
T_{out}	Air outlet temperature, ℃
T_{pl}	Perforated plate temperature, ℃
T_a	Ambient temperature, ℃
Cp	Specific heat of air, $J/kg \cdot K$
G	Solar radiation intensity, W/m^2
A_S	Collector surface area, m^2
$\dot{m}$	Air mass flow rate, kg/s
Q_{th}	Useful heat energy, W
P_{el}	Electrical output power, W
V	Voltage output, V
I	Current output, A
C_0	Capital Cost
C_{PV}	Cost of panel
$C_{thermal}$	Cost of thermal collector
C_{blower}	Cost of centrifugal blower
$C_{structure}$	Cost of Structure
$C_{installation}$	Labor & installation cost
$C_{inverters}$	Cost of inverters
C_{OP}	Annual Operating Cost
$Q_{heating}$	Daily consumption for space heating
E_a	annual energy produced, kWh/year
EF	$CO_2 emission\ factor$, $kgCO_2$ /kWh
ω_P	Uncertainty of Photovoltaic power
ω_{th}	Uncertainty of thermal power

Greek Symbols

η_{th}	Thermal efficiency, %
η_{el}	Electrical efficiency, %
$\eta_{overall}$	Overall efficiency, %
ε	Surface emissivity
σ	Stefan − Boltzman constant, $W/m^2.K^4$
ρ	Air density, kg/m^3

Abbreviation

PV	Photovoltaic
PVT	Photovoltaic Thermal System
LCOE	Levelized Cost of Energy
NPV	Net Present Value
SD card	Secure Digital Card
RTC	Real-Time Clock
UNO	Arduino Uno Microcontroller
DS18B20	Digital Temperature Sensor
HDD	Heating Dgree Day

REFERENCE

[1] G. Prakash, H. Anuta, D. Gielen, R. Gorini, N. Wagner, and G. Gallina, "Future of wind: Deployment, investment, technology, grid integration and socio-economic aspects (A Global Energy Transformation paper)," *Renew. Energy Agency*, 2019, [Online]. Available: https://www.irena.org/-/media/Files/IRENA/Agency/Publication/2019/Oct/IRENA_Future_of_wind_2019.pdf

[2] M. H. Shubbak, "Advances in solar photovoltaics : Technology review and patent trends," *Renew. Sustain. Energy Rev.*, vol. 115, no. July, p. 109383, 2019, doi: 10.1016/j.rser.2019.109383.

[3] W. Bank, "Electricity Services Reconstruction and Enhancement Project," 2019, [Online]. Available: http://documents.worldbank.org/curated/en/504001557108087756/pdf/Iraq-Electricity-Services-Reconstruction-and-Enhancement-Project.pdf

[4] I. E. Agency, "A Roadmap to a Brighter Future Iraq ' s Energy Sector," *Int. Energy Agency*, no. April, 2019, [Online]. Available: https://www.iea.org/reports/iraqs-energy-sector-a-roadmap-to-a-brighter-future

[5] O. Rafae, N. Moneer, O. Mohammed, A. Salih, N. M. Abdulrazzaq, and S. M. Samad, "Energetic , economic environmental analysis for photovoltaic grid-connected systems under different climate conditions in Iraq," *Clean. Energy Syst.*, vol. 10, no. February, p. 100180, 2025, doi: 10.1016/j.cles.2025.100180.

[6] J. D. Nrel, P. M. Nrel, L. L. Nrel, J. B. Nrel, and D. J. Group, "Photovoltaic-Thermal New Technology Demonstration," no. January, 2015, [Online]. Available: https://www.nrel.gov/docs/fy15osti/63474.pdf

[7] Ã. Aste, G. Chiesa, and F. Verri, "Design , development and performance monitoring of a photovoltaic-thermal (PVT) air collector," *Renew. energy*, vol. 33, no. 5, pp. 914–927, 2008, doi: 10.1016/j.renene.2007.06.022.

[8] S. A. Brideau and M. R. Collins, "Experimental model validation of a hybrid PV/thermal air based collector with impinging jets," *Energy Procedia*, vol. 30, pp. 44–54, 2012, doi: 10.1016/j.egypro.2012.11.007.

[9] I. Bizzy and L. Mustafrizal, "PV Panel

Cooler to Enhance Output Performance Using Perforated Aluminium Plate," *J. Phys. Conf. Ser.*, vol. 1198, no. 4, 2019, doi: 10.1088/1742-6596/1198/4/042003.

[10] I. Bizzy, R. Sipahutar, D. Puspitasari, A. Sofijan, and M. A. Fajri, "The cooling effect of polycrystalline type PV panels using perforated aluminum plates," *IOP Conf. Ser. Mater. Sci. Eng.*, vol. 909, no. 1, p. 12005, 2020, doi: 10.1088/1757-899X/909/1/012005.

[11] A. Brideau and M. R. Collins, "ScienceDirect Development and validation of a hybrid PV / Thermal air based collector model with impinging jets," *Sol. Energy*, vol. 102, pp. 234–246, 2014, doi: 10.1016/j.solener.2014.01.022.

[12] J.-H. Kim, J.-S. Yu, and J.-T. Kim, "An experimental study on the energy and exergy performance of an air-type PVT collector with perforated baffle," *Energies*, vol. 14, no. 10, p. 2919, 2021, doi: 10.3390/ en14102919.

[13] M. Fterich, H. Chouikhi, H. Bentaher, S. Sandoval-Torres, and A. Maalej, "Efficiency Analysis of Photo-Voltaic Thermal Air Collectors," in *2019 International Conference on Power Generation Systems and Renewable Energy Technologies (PGSRET)*, IEEE, 2019, pp. 1–6. doi: 10.1109/PGSRET.2019.8882658.

[14] R. Mazón-Hernández, J. R. García-Cascales, F. Vera-García, A. S. Káiser, and B. Zamora, "Improving the electrical parameters of a photovoltaic panel by means of an induced or forced air stream," *Int. J. Photoenergy*, vol. 2013, no. 1, p. 830968, 2013, doi: 10.1155/2013/830968.

[15] I. Baklouti and Z. Driss, "Numerical and Experimental Study of the Impact of Key Parameters on a PVT Air Collector: Mass Flow Rate and Duct Depth," *J. Therm. Sci.*, vol. 30, no. 5, pp. 1625–1642, 2021, doi: 10.1007/s11630-020-1345-8.

[16] O. R. Alomar, O. M. Ali, B. M. Ali, V. S. Qader, and O. M. Ali, "Energy, exergy, economical and environmental analysis of photovoltaic solar panel for fixed, single and dual axis tracking systems: An experimental and theoretical study," *Case Stud. Therm. Eng.*, vol. 51, no. October, p. 103635, 2023, doi: 10.1016/j.csite.2023.103635.

[17] J. P. Holman, *Experimental methods for engineers eighth edition*. 2021. [Online]. Available: https://www.mheducation.com/highered/product/experimental-methods-engineers-holman/M9780073529301.html

[18] J. A. Duffie and W. A. Beckman, *Solar engineering of thermal process*, vol. 2. John Wiley & Sons, Inc., 2013. [Online]. Available: https://www.sku.ac.ir/Datafiles/BookLibrary/45/…pdf

[19] Y. Cengel and A. Ghajar, *Heat and mass transfer: fundamentals and applications McGraw-Hill*, Six editio. McGraw-Hill Education, 2014. [Online]. Available: https://www.mheducation.com/highered/product/heat-mass-transfer-fundamentals-applications-cengel-ghajar/M9780073398181.html

[20] S. A. Zubeer and O. M. Ali, "Experimental and numerical study of low concentration and water-cooling effect on PV module performance," *Case Stud. Therm. Eng.*, vol. 34, no. April, p. 102007, 2022, doi: 10.1016/j.csite.2022.102007.

[21] E. Arslan, M. Aktaş, and Ö. F. Can, "Experimental and numerical investigation of a novel photovoltaic thermal (PV/T) collector with the energy and exergy analysis," *J. Clean. Prod.*, vol. 276, 2020, doi: 10.1016/j.jclepro.2020.123255.

[22] A. Audenaert, L. De Boeck, S. De Cleyn, S. Lizin, and J. F. Adam, "An economic evaluation of photovoltaic grid connected systems (PVGCS) in Flanders for companies: A generic model," *Renew. Energy*, vol. 35, no. 12, pp. 2674–2682, 2010, doi: 10.1016/j.renene.2010.04.013.

[23] O. M. Ali, O. R. Alomar, and S. I. Mohamed, "Technical, economical and environmental feasibility study of a photovoltaic system under the climatic condition of north Iraq," *Int. J. Ambient Energy*, vol. 44, no. 1, pp. 212–220, 2023, doi: 10.1080/01430750.2022.2126004.

[24] A. S. Alaboodi and S. J. Alharbi, "A Study on the Techno-Economics Feasibility of a 19.38 KWp Rooftop Solar Photovoltaic System at Al-Abrar Mosque, Saudi Arabia," *Energies* , vol. 17, no. 10, 2024, doi: 10.3390/en17102325.

[25] A. K. Saxena, S. Saxena, and K. Sudhakar, "Energy, economic and environmental performance assessment of a grid-tied rooftop system in different cities of India based on 3E analysis," *Clean energy*, vol. 5, no. 2, pp. 288–301, 2021, doi: 10.1093/ce/zkab008.

[26] S. K. Al-Mosawy, S. M. Al-Jawari, and I. J. Al-Yassri, "Estimation of domestic

urban electricity consumption: A case study of Baghdad, Iraq," *Period. Eng. Nat. Sci.*, vol. 9, no. 2, pp. 678–683, 2021, doi: 10.21533/pen.v9i2.1869.

[27] V. Tan, P. R. Dias, N. Chang, and R. Deng, "Estimating the Lifetime of Solar Photovoltaic Modules in Australia," *Sustain.*, vol. 14, no. 9, 2022, doi: 10.3390/su14095336.

[28] M. Baban, "Iraq and the Kurdistan Region : Divergent Approaches to Electricity," pp. 1–15, 2025, [Online]. Available: https://rudawrc.net/en/article/iraq-and-the-kurdistan-region-divergent-approaches-to-electricity-supply-2025-05-18

[29] A. E. Kabeel, M. Abdelgaied, and R. Sathyamurthy, "A comprehensive investigation of the optimization cooling technique for improving the performance of PV module with re fl ectors under Egyptian conditions," vol. 186, no. May, pp. 257–263, 2019, doi: 10.1016/j.solener.2019.05.019.